Determining Absolute Electrochemiluminescence Efficiencies of Two Iridium Complexes**

Liuqing Yang[†a], Jonathan R. Adsetts[†a], Ruizhong Zhang[†a,d], Barbora Balónová[b], Marta T. Piqueras[b], , Kenneth Chu[a], Congyang Zhang[a], Eli Zysman-Colman[c,], Barry A. Blight[b,*], Zhifeng Ding[a,*]*

[a] Department of Chemistry, Western University, London, ON, Canada, N6A 3K7. E-mail: zfding@uwo.ca.

[b] Department of Chemistry, University of New Brunswick, Fredericton, NB, Canada, E3A 5A3. E-mail: b.blight@unb.ca

[c] Organic Semiconductor Centre, EaStCHEM School of Chemistry, University of St Andrews, St Andrews, Fife, UK, KY16 9ST. E-mail: eli_journals@zysman-colman.com

[d] Department of Chemistry, Tianjin University, Tianjin, China. E-mail: zhangrz2019@tju.edu.cn

(†) Authors equally contributed.

** Dedicated to Prof. Shaojun Dong for her pioneering research on modern electrochemistry on the occasion of her 90th birthday.

ABSTRACT:

This work reports the absolute electrochemiluminescence (ECL) quantum efficiencies (QEs) of two iridium(III) complexes, ***fac*-Ir(ppy)$_3$** (**Ir-1**) and **[Ir(ppy)$_2$(dtbubpy)]$^+$** (**[Ir-2]$^+$**) in annihilation and coreactant pathways. With potentiodynamic scans and potential pulsing, ECL mechanisms were investigated by means of ECL-voltage curves, ECL-time curves and ECL spectroscopy. It was demonstrated that the radical stability and reactivity are the two main factors affecting ECL efficiencies in various processes, while intermediate charges have little effect. Considering the difference of such radical behaviors between $[Ru(bpy)_3]^{2+}$ and other luminophores, absolute ECL QE is more applicable compared with the ones relative to $[Ru(bpy)_3]^{2+}$ as a standard.

Keywords: *Iridium(III) complexes, Electrochemiluminescence, Absolute and relative quantum efficiency, Radical stability, Radical reactivity*

1. Introduction

Smartly combining electrochemistry and chemiluminescence, electrochemiluminescence (ECL) or electrogenerated chemiluminescence, is a light emission process that occurs from the electron transfer between highly active radical species that are electrochemically generated[1-3]. ECL has become an essential modern electroanalytical technique with wide applications in the fields of biosensing[4-6], bioimaging[7-9], and immunoassays[10-12]. Furthermore, ECL investigation can also provide guidelines for light-emitting electrochemical cells (LECs) who has similar luminescent mechanisms. Many ECLphores have been reported including organic molecules[13-15], organometallic complexes[16-18] and nanomaterials[19-21]. The most important factor that determines the ECL performance of a compound is the ECL quantum efficiency (QE), which is defined as the ratio of the number of photons emitted to the number of electrons injected during an ECL process[22, 23]. However, unlike the absolute photoluminescence quantum yield (PLQY), which is defined as the number of photons emitted by the number of photons absorbed and can be measured directly in an integrating sphere, absolute ECL QEs have been rarely reported. The Bard group reported the absolute ECL QE of $[Ru(bpy)_3]^{2+}$ from an annihilation pathway as 5% using a photodiode and actinometry using a platinum rotating ring-disk electrode (RRDE)[24]. The Bard group also reported the absolute ECL QE of 9,10-diphenylanthracene (DPA), thianthrene (TH) and other systems, with values ranging from 1.5%-20%[25]. Recently, our group used a calibrated photomultiplier tube (PMT) to determine the absolute ECL QE of $[Ru(bpy)_3]^{2+}$ via a annihilation route with either potentiodynamic scans or potential pulsing, obtaining, respectively, 0.0019%, and 0.090%-2.4% ECL QE, which are close to Bard's results[22]. Our group also employed a photon-counting device to measure the absolute ECL QE of the $[Ru(bpy)_3]^{2+}$/tri-*n*-propylamine (TPrA) system, obtaining 10.0 ± 1.0% using potential pulsing at 10 Hz, a value that is greatly enhanced from that in the annihilation pathway[23].

Instead of reporting the absolute ECL QE, many research groups including ours have utilized the 5% $[Ru(bpy)_3]^{2+}$ as a standard to determine the relative QEs during ECL studies[26-31]. The relative ECL QE determination is easy to undertake, and it provides some information regarding the relative ECL performance of the compound of interest. However, this methodology cannot be generalized as this value is not valid if the experimental conditions are not identical to aforementioned approaches. More importantly, it is essential to recognize that the stability and reactivity of the radical species during the ECL processes are likely to be different between $[Ru(bpy)_3]^{2+}$ and other ECL materials. Without considering such factors, the investigation of relative QEs makes less sense compared with absolute determination. Elucidation of absolute ECL QE of other materials remains in great demand.

Iridium(III) complexes have occupied a central role in many photonics and optoelectronic applications due to their high efficiency, tunable emission, and short excited state lifetime[32-35], properties that also contributed to their use as bright ECLphores[18, 30, 36-38]. Determining the absolute ECL QE of iridium(III) complexes has to date not been reported and quantification of

such efficiencies is necessary to better understand the insight into ECL mechanisms and employ these complexes in practical ECL applications. Herein, we report the absolute ECL QEs of two known iridium(III) complexes, *fac*-Ir(ppy)$_3$ (**Ir-1**) and [Ir(ppy)$_2$(dtbubpy)] ·PF$_6$ (**[Ir-2]**$^+$), using both potentiodynamic scans and potential pulsing. The structures of the two complexes are displayed in Fig. 1.

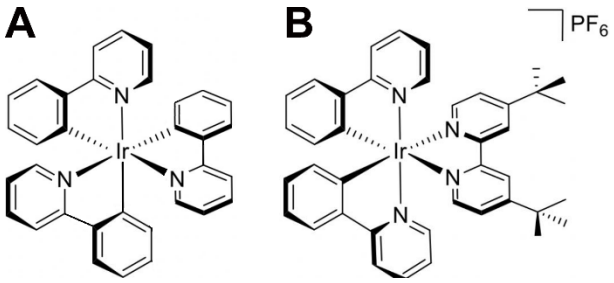

Fig. 1. Structures of (A) *fac*-Ir(ppy)$_3$ (**Ir-1**) and (B) [Ir(ppy)$_2$(dtbubpy)]·PF$_6$ (**[Ir-2]**$^+$).

2. Experimental

2.1. Chemicals and reagents

Acetonitrile (MeCN, anhydrous, 99.8%), tetrabutylammonium hexafluorophosphate (TBAPF$_6$, for electrochemical analysis, ≥99.0%), benzoyl peroxide (BPO, reagent grade, ≥98%) and ferrocene (Fc, 98%) were all purchased from Sigma-Aldrich (Mississauga, ON, Canada). MeCN was received in a Sure/Seal^{TM} bottle and directly transferred to the N_2 filled glove box. BPO was stored in a refrigerator at 4 °C. The synthesis of **Ir-1** and **[Ir-2]**$^+$ were reported elsewhere[39, 40].

2.2. ECL Methods

A three-electrode system was utilized for the ECL experiments, consisting of a 2 mm platinum (Pt) disk in a glass sheath as working electrode and two Pt wire coils as counter and reference electrodes. The Pt working electrode was manually polished with 0.3 μm and 0.05 μm Al_2O_3 suspensions on a polishing pad. A mirror-like surface should be obtained. Then it was electrochemically polished in 0.1 M H_2SO_4 solution by scanning potentials between -0.30 V and 1.25 V for 400 cycles. Then the Pt working electrode was thoroughly rinsed with water and dried with argon gas blowing. The two Pt wires were successively sonicated in acetone, isopropanol and water then dried at 120 °C in an oven.

ECL experiments were performed in a glass electrochemical cell. The bottom of the cell was a specifically designed flat Pyrex window that allows the ECL signal pass through to be detected. The cell was thoroughly rinsed with acetone, isopropanol and water, successively immersed for four hours each in 5% KOH and 1% HCl baths, and it was rinsed again with amounts of water before it was dried at 120 °C in an oven.

Prior to the ECL experiments, the luminophore and supporting electrolyte $TBAPF_6$ were placed in the electrochemical cell, which was brought into the N_2 filled glove box together with the three-electrodes. The solvent MeCN was added into the cell in the glove box and then the whole system was assembled together and sealed tightly. During the experiments, the electrochemical cell was set in a custom designed black box covered with a black film bag to reduce any background light interference. After the ECL experiments, Fc was added to the system as an internal potential reference to calibrate the applied potentials to SCE. (The formal potential $E_{Fc+/Fc}^{0'}$ was taken as 0.38 V vs. SCE in MeCN)[18].

2.3. ECL Instrumentation

For the measurements of CV and ECL-voltage curves during potential scans, current-time and ECL-time curves during potential pulsing experiments, an Autolab potentiostat (PGSTAT30, Metrohm, Switzerland) controlled by its NOVA software was used as the ECL driving force[22]. A photomultiplier tube (PMT, R3869, Hamamatsu, Japan) biased at -750 V by a high voltage supply was used to detect ECL signals generated in the vicinity of the working electrode. A picoammeter (Keithley 6487, Cleveland, OH) was employed to transform the photocurrent as the ECL intensity detected by the PMT to a voltage signal which was fed into one of the two auxiliary ports of the Autolab and displayed as an external signal in the NOVA software. The sensitivity on the picoammeter was manually adjusted to avoid its display saturation. All the other parameters were also accordingly adjusted in the NOVA software. As introduced in section 2.2, the electrochemical cell was placed in the black box above the PMT during the whole experiments, maintaining a constant distance of 7.37 cm between the working electrode surface and PMT window.

For the ECL spectroscopy measurements[41], a CHI610A electrochemical workstation (CH Instruments, Austin, TX) was utilized as ECL driving force. The electrochemical cell was placed above a spectrograph with a grating of 50 l/mm blazed at 600 nm (Acton 2300i, Teledyne Princeton Instruments, Trenton, NJ) coupled with a CCD camera (Model DU401-BR-DD-352, Andor Technology, UK). Prior to any spectroscopy capture, the CCD camera was cooled down to -65 ℃ and calibrated with a HG-1 mercury-argon source (Ocean Optics, Orlando, FL). All the electrochemistry parameters were adjusted in the CHI software while the ones of spectroscopy measurements were controlled by the corresponding Andor Technology program.

3. Results and discussion

3.1. ECL efficiencies determination

Absolute ECL quantum efficiency is defined as the number of photons emitted by the number of electrons injected as indicated in equation (1), where ν_{photon} is the total photon emission rate which can be converted from the photocurrent detected by the PMT, and $\nu_{electron}$ is the total Faradaic

electron injection rate that is determined by subtraction of non-Faradaic current from the total current measured[22].

$$\emptyset_{ECL} = \frac{\int \nu_{photon} dt}{\int \nu_{electron} dt} \times 100\% \quad (1)$$

Many factors must be considered to convert photocurrent to ν_{photon}:

1. ECL detection correction: During the ECL measurement, some of the light generated in the vicinity of the electrodes were not detected by the PMT, and a correction factor σ_{PMT} is introduced considering the PMT surface area (A_{PMT}), distance from PMT to electrode (d), and electrode reflectivity (R) which is defined in equation (2).

$$\sigma_{PMT} = \frac{A_{PMT}}{4\pi d^2} \times (1 + R) \quad (2)$$

2. Hardware and wavelength specific factor: Considering the difference of PMT's sensitivity to ECL emission at specific wavelength, a hardware and wavelength specific factor (C) is introduced as seen in equation (3) after the calibration of PMT,

$$C = \frac{\int Q(\lambda) S(\lambda) d\lambda}{\int S(\lambda) d\lambda} \quad (3)$$

where $Q(\lambda)$ is the calibrated quantum efficiency of PMT (electrons per photon) while $S(\lambda)$ is the normalized ECL emission spectrum with background subtraction.

3. Self-absorption correction: During the ECL process, the iridium complexes in solution could self-absorb the ECL emitted. The absorption correction factor (k_{ABS}) as shown in equation (4), is determined from the UV-Vis absorption spectrum and ECL emission spectrum, which method is outlined in our previous report[22].

$$k_{ABS} = \frac{\int total\ Emission\ d\lambda + \int absorbed\ Emission\ d\lambda}{\int total\ Emission\ d\lambda} \quad (4)$$

With the corrections considered above, the total photon emission rate ν_{photon} can be converted from the photocurrent (PC) detected by the PMT by equation (5), where N_A and F represent Avogadro's number and Faraday's constant, respectively.

$$\nu_{photon} = \frac{PC \times N_A \times k_{ABS}}{F \times \sigma_{PMT} \times C} \quad (5)$$

Furthermore, unlike Faradaic current, the non-Faradaic current during an electrochemistry process does not contribute to the ECL generation and needs to be subtracted when determining the absolute ECL efficiency. Determination of Faradaic current (i_F) is shown in equation (6), where i_{BG} indicates the background current (non-Faradaic current) and i_x represents the total current (Faradaic and non-Faradaic current). Note that for the co-reactant ECL route, most of the electrons are injected into the system to reduce the co-reactant BPO. However, the reduction of BPO is necessary in the whole ECL generation process, and the current of such reduction should be considered as "Faradaic current" although it is not related to the initial redox of the main ECL luminophore.

As introduced in our recent publication[22], the background current measurements were performed simultaneously with the ECL tests, with potentials applied right below the oxidation and/or reduction of the species where ECL has not been generated yet. All the other test conditions remain the same.

$$i_F = i_x - i_{BG} \quad (6)$$

Then the total Faradaic electron injection rate $\nu_{electron}$ is determined by equation (7), where i_F is the Faradaic current from equation (6) and q_e is a constant related to the charges per electron:

$$\nu_{electron} = \frac{i_F}{q_e} \quad (7)$$

As such, combining equation (1), (5) and (7), absolute ECL efficiencies are determined from the photocurrent (PC) and current (i_x) using equation (8):

$$\emptyset_{ECL} = \frac{\int PC\ dt}{\int (|i_x| - |i_{BG}|)\ dt} \times \frac{N_A \times k_{ABS} \times q_e}{F \times \sigma_{PMT} \times C} \quad (8)$$

The parameters for the calculations are summarized in the Supporting Information (Table S1) and Matlab codes employed are the same as our previous report [22]. In this work, we have applied potentialdynamic method at a scan rate of 100 mV/s (CV-ECL), potential pulsing at 10 Hz, and 100 Hz, respectively, to **Ir-1** and **[Ir-2]**$^+$ and determined their absolute ECL efficiencies. The results are shown in Table 1, and are further discussed in the following sections.

Table 1. Absolute and relative ECL efficiencies of **Ir-1** and **[Ir-2]**$^+$.

Absolute and Relative ECL Efficiencies						
Method	**CV-ECL**		**Pulsing at 10 Hz**		**Pulsing at 100 Hz**	
	Absolute	**Relative**	**Absolute**	**Relative**	**Absolute**	**Relative**
Ir-1_Ann	0.0013%	3.8%	0.039%	1.4%	0.17%	0.85%
$[Ir\text{-}2]^+$_Ann	0.0016%	9.7%	0.072%	1.6%	0.22%	1.4%
Ir-1_BPO	0.027%	1.7%	0.65%	2.2%	0.86%	1.8%
$[Ir\text{-}2]^+$_BPO	0.37%	13%	1.4%	3.5%	2.2%	2.6%

3.2. ECL during potentiodynamic scans

Fig. 2 displays the CVs with the corresponding ECL-voltage curves of 0.5 mM **Ir-1** (Fig. 2A) and **[Ir-2]**$^+$ (Fig. 2B) in MeCN at a scan rate of 0.1 V/s. **Ir-1** undergoes an oxidation reaction and a reduction reaction at peak potentials of 0.57 V and -2.31 V, respectively, and generates ECL in both anodic and cathodic scans. It should be noted that in this annihilation pathway, the anodic ECL of **Ir-1** is much stronger than the cathodic one. In comparison, the oxidation and reduction

potentials of **[Ir-2]**$^+$ are located at 1.36 V and -1.48 V, respectively, both of which are more anodically shifted than those of **Ir-1**. As seen in the purple curve in Fig. 2B, **[Ir-2]**$^+$ produces no appreciable anodic ECL but high cathodic ECL (~45 nA) in the annihilation route, which is much stronger than the cathodic ECL of **Ir-1** (~3 nA). It is plausible that the iridium atom in **[Ir-2]**$^+$ bonded with N has greater metal character than the one bonded with C in **Ir-1**, which produces a more chemically stable oxidation, thus allowing enough time for the radical dications to diffuse and interact with the neutral radicals in the vicinity of the working electrode to produce ECL[42].

During the potential scans, accumulated ECL spectra of both samples were acquired as shown in Fig. S1. Combined with the absorption corrections (Fig. S2 and Table S1), they were employed to determine the C factor[22] together with the PMT responsivity curve (Fig. S3 and Fig. S4). The absolute ECL efficiencies from Fig. 2 were thereafter determined to be 0.0013% for **Ir-1**, and 0.0016% for **[Ir-2]**$^+$ (Table 1), both of which are comparable with that of $[Ru(bpy)_3]^{2+}$ (0.0019%) via an annihilation ECL pathway during CVs as previously reported by our group[22].

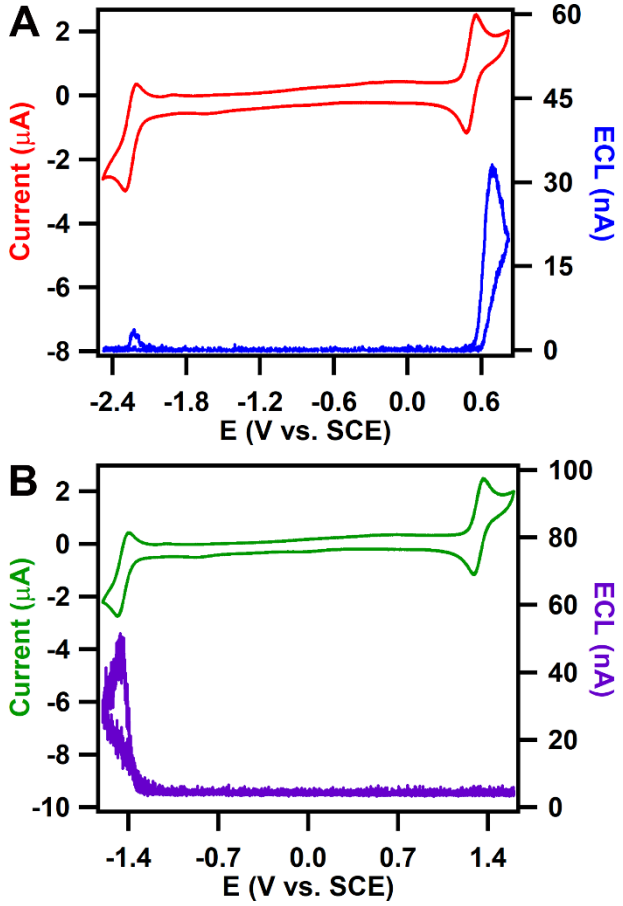

Fig. 2. CVs with the corresponding ECL-voltage curves of 0.5 mM (A) **Ir-1** and (B) **[Ir-2]**$^+$ acquired in MeCN at a scan rate of 0.1 V/s.

Benzoyl peroxide (BPO) was then added as an oxidative coreactant to improve the ECL performances. It should be noted that the ECL of **Ir-1** and **[Ir-2]**$^+$ in the annihilation route, and

that of **Ir-1** with TPrA as the coreactant were previously reported by other groups and us[18, 37, 43]. However, the ECL behavior of these two iridium complexes have never been investigated with a reduction-oxidative coreactant like BPO. Fig. 3A and 3B illustrate the CVs with corresponding ECL-voltage curves of 0.5 mM **Ir-1** and **[Ir-2]**$^+$ in MeCN with the addition of 5 mM BPO, respectively. The onset of the ECL potential of **Ir-1**/BPO system is at -2.12 V, right at the reduction of **Ir-1**, approaching a maximum ECL intensity of 31 µA. Similarly, the onset ECL of the **[Ir-2]**$^+$/BPO solution is located at -1.41 V, which is also close to the reduction of **[Ir-2]**$^+$. The ECL intensity of the latter system reaches up to 148 µA, which is much higher than the **Ir-1** system. The absolute ECL efficiencies of the two iridium complexes-BPO systems during CVs were then determined (Table 1). The ϕ_{ECL} of **[Ir-2]**$^+$ is 0.37%, which is more than 10 times higher than that of **Ir-1**, 0.027%.

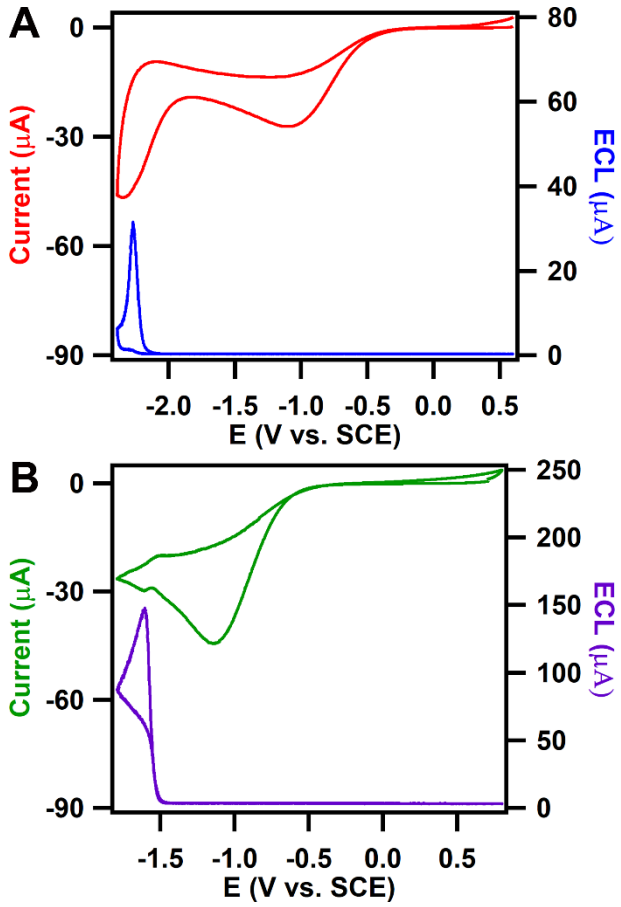

Fig. 3. CVs with the corresponding ECL-voltage curves of 0.5 mM (A) **Ir-1** and (B) **[Ir-2]**$^+$ with 5 mM BPO as the coreactant acquired in MeCN at a scan rate of 0.1 V/s.

For both iridium complexes, the coreactant pathway shows higher efficiencies than the annihilation pathway. This is because both the iridium complexes and coreactant BPO were reduced close to each other within negative potential regions, thus the ratio of decayed radicals is smaller while the amounts of radicals to produce ECL are increased. Furthermore, the benzoate radical (PhCOO·) is

quite a strong oxidant, thus shows much higher reactivity than the radicals of the iridium complexes, so it can preferentially take an electron from the iridium complexes to generate their excited states[1].

In contrast, the **[Ir-2]**$^+$/BPO coreactant system demonstrates higher ECL efficiencies than that of **Ir-1**/BPO, while the annihilation ECL efficiencies of the two luminophores are very close (0.0013% for **Ir-1**, and 0.0016% for **[Ir-2]**$^+$). The stability and reactivity of radicals could perfectly explain these observations: For annihilation, the generation of ECL requires both the radical cations and radical anions (radical dications and neutral radicals for **[Ir-2]**$^+$ since it carries one positive charge initially). The potential difference between the redox of **Ir-1** and **[Ir-2]**$^+$ is close. With the same scan rate of 0.1 V/s in CVs scans, it results in similar time for radicals of **Ir-1** (33.6 s) and **[Ir-2]**$^+$ (32.3 s) to interact and recombine with their counterpart, respectively. The CV scan durations are quite long compared with the lifetime of radicals. As such, the kinetic stability of radicals is the key factor for ECL efficiency in the annihilation route. Based on their similar efficiencies, it is plausible that the stability of **Ir-1** and **[Ir-2]**$^+$ radicals are close. For the BPO co-reactant process, ECL emission requires the reduction of both BPO and the iridium complexes. As shown in the CVs (Fig. 3), BPO is always reduced first at -1.10 V, while **Ir-1** is reduced at -2.31 V and **[Ir-2]**$^+$ is reduced at -1.48 V. At a scan rate of 0.1 V/s, it takes 12.1 s for BPO radicals to encounter the **Ir-1** radicals, while most of the BPO radicals would have decayed during this time period. On the contrary, only 3.8 s is required for the interactions between BPO and **[Ir-2]**$^+$ radicals, meaning that relatively fewer BPO radicals would have decayed and thus can react with the **[Ir-2]**$^+$ radicals to generate ECL. Noting that the onset of the ECL occurs right at the potential of the reduction of the iridium complexes, the intrinsic stability of reduced iridium complex radicals is no longer an issue. This explains well that the ECL efficiency of **[Ir-2]**$^+$ is much higher than that of **Ir-1** despite the lower photoluminescence quantum yield through the co-reactant mechanism with BPO.

3.3. Spooling ECL spectroscopy

Spooling ECL spectroscopy was developed by our group, which is employed to reveal the kinetics of the ECL[41]. Fig. 4 displays the spooling ECL spectra of **Ir-1** and **[Ir-2]**$^+$ acquired within CV scans upon addition of 5 mM BPO as the coreactant. The spectra of both samples are color coded to distinguish the evolution and devolution of the ECL processes based on which two mechanisms are proposed as described in Chart 1. Taking **Ir-1** as an example, after the reduction of BPO, a strongly oxidizing benzoyl radical (PhCOO·) is generated. In one pathway, this species could oxidize the radical anion of **Ir-1** generated at -2.12 V to produce the **Ir-1*** that emits ECL right at -2.12 V (Chart 1A). Alternatively, PhCOO· could also oxidize the neutral **Ir-1**, producing radical cations of **Ir-1** that could thereafter react with the radical anions of **Ir-1** to emit ECL at -2.12 V (Chart 1B). In both mechanisms, ECL is generated at -2.12 V where the **Ir-1** radical anions are produced. The onset ECL potentials and ECL regions revealed by the spooling ECL spectroscopy match well with the ECL-voltage curves in Fig. 3.

As seen in the insets of Fig. 4, the spectra of both iridium complexes display constant shapes and peak wavelengths during potential scans, indicating the independence of the excited states on applied potentials. Furthermore, the spectra also demonstrated the same features as their annihilation ECL spectra (Fig. S1), providing evidence that identical excited states are generating ECL during annihilation and coreactant processes.

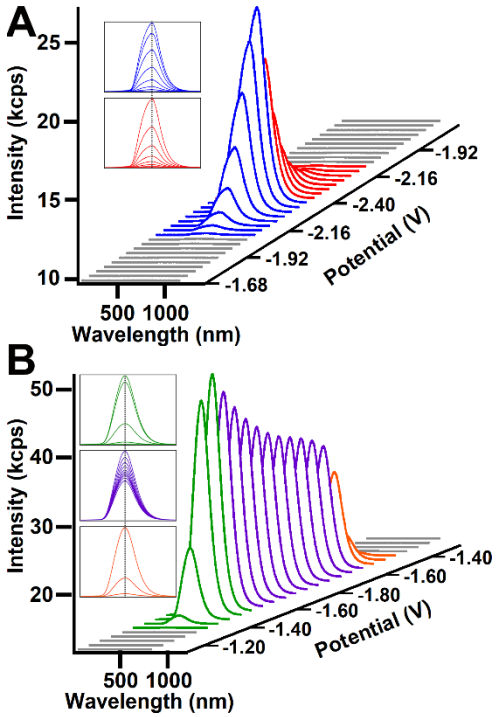

Fig. 4. Spooling ECL spectra of 0.5 mM (A) **Ir-1** and (B) **[Ir-2]**$^{+}$ with 5 mM BPO as the coreactant during a CV scan. Insets are the 2D views of spooling ECL spectra demonstrating constant shapes and peak wavelengths.

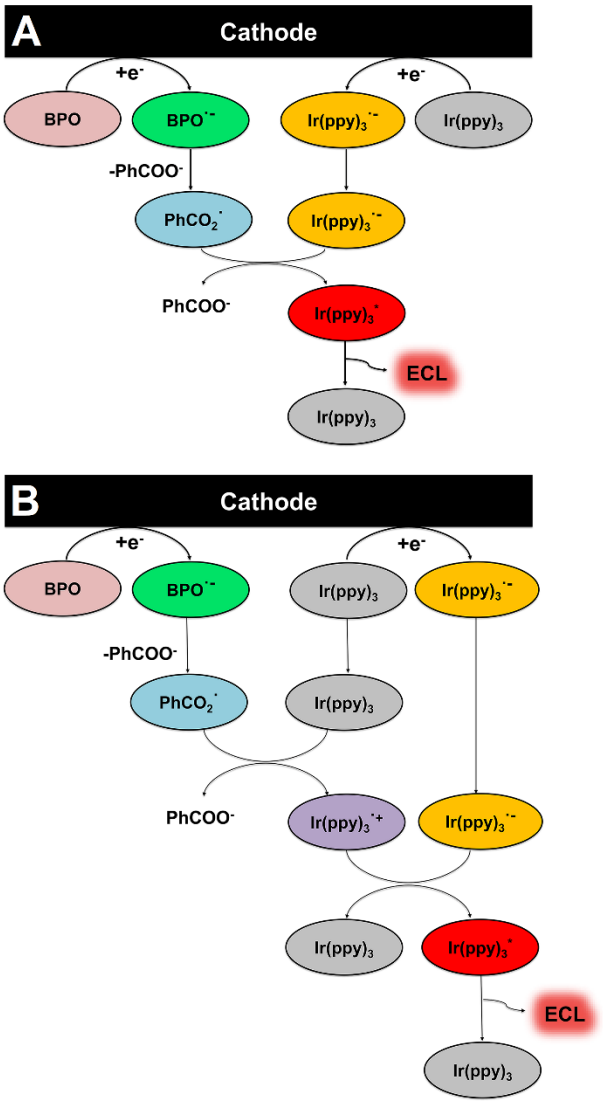

Chart 1. ECL mechanisms of ***fac*-Ir(ppy)$_3$ (Ir-1)** with BPO as coreactant.

3.4. ECL during potential pulsing

Compared with CV-ECL, potential pulsing ECL experiments can significantly reduce the time delay for the radicals to meet, react and generate ECL. Fig. 5A and Fig. 5B, respectively, display three cycles of current-time with the corresponding ECL-time curves of 0.5 mM **Ir-1** and **[Ir-2]**$^+$ via an annihilation pathway during a potential pulsing between their redox potentials at 10 Hz. Absolute efficiencies were also determined for the pulsed-ECL. In fact, Fig. 5 only illustrates three cycles during the whole processes. Fig. S5 shows the ECL-time curves of both **Ir-1** and **[Ir-2]**$^+$ in different routes for the entire potential pulsing processes, based on which total electrons flux (electrons per second) and total photons flux (photons per second) were determined, as introduced in section 3.1 as well as documented in our previous report[22]. Such flux curves of **[Ir-2]**$^+$ during an annihilation process at 10 Hz are shown in Fig. S6 as an example.

As the pulsing frequency was set at 10 Hz, the time interval between the generation of radical cations and anions was set to 0.1 s, which is significantly faster than that in a CV-ECL experiment at a scan rate of 0.1 V/s. As a result, compared with the ECL-voltage curves during CVs in Fig. 2, their ECL intensities increase more than 200 times, approaching ~10 μA. The ECL efficiencies also increased from 0.0013% to 0.039% for **Ir-1**, and from 0.0016% to 0.072% for **[Ir-2]**$^+$, respectively, thanks to the much shorter time interval between the formation of their radical cations and anions. Interestingly, during CV scans, **Ir-1** demonstrates higher ECL under positive potentials (Fig. 2A), while with potential pulsing it shows much higher ECL at negative potentials (Fig. 5A). This is because in a scanning ECL process, the stability of the radicals dominates, while in a pulsing ECL process, the frequency is set to be constant and the influence of the intrinsic reactivity of the radicals on the ECL becomes dominant. It is plausible that the stability of the **Ir-1** radical anions is higher, but their reactivity is lower than the radical cations of **Ir-1**.

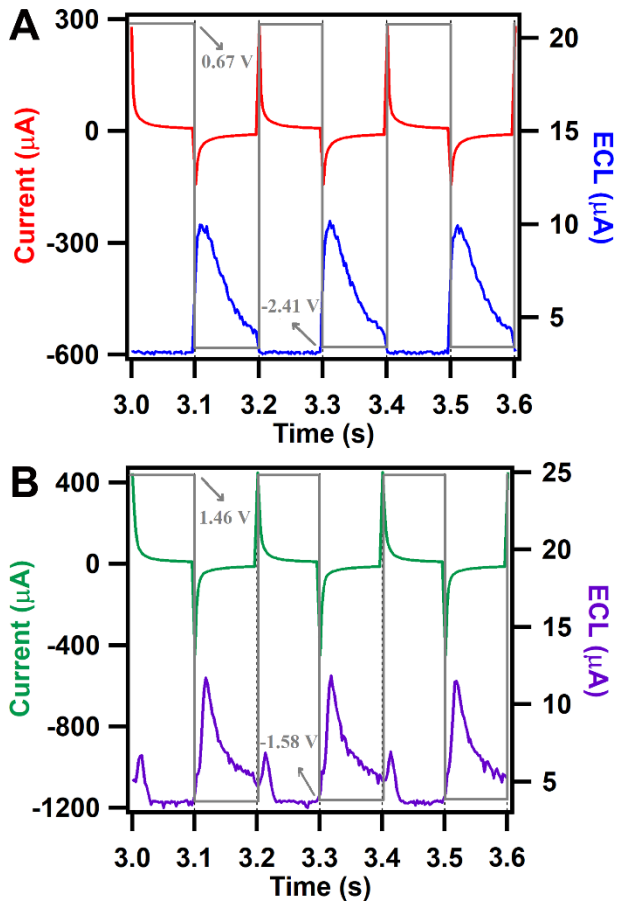

Fig. 5. Three cycles of current-time with the corresponding ECL-time curves of 0.5 mM (A) **Ir-1** and (B) **[Ir-2]**$^+$ during a potential pulsing experiment at 10 Hz frequency. The corresponding applied potentials are indicated in grey.

When BPO was added as a coreactant, the potentials were pulsed between 0.58 V and their ECL peak potentials as shown in Fig. 6. Once more, the two iridium complexes demonstrate higher ECL efficiencies (seen in Table 1) compared with both their CV-ECL in the coreactant route (Fig. 3) thanks to the smaller time interval, and their pulsed-ECL in annihilation process (Fig. 5) thanks to BPO. Notably, the pulsed-ECL of **[Ir-2]**$^+$ with 5 mM BPO (Fig. 6B) was so strong that it saturated the PMT and an optical filter (OD=1) was placed in front of the PMT window to avoid saturation. Thus, the ECL intensity shown in Fig. 6B is in fact 10 times smaller than it truly performed. Also noteworthy is the fact that that **Ir-1** generates ECL immediately when the potential is switched (Fig. 6A), while there is an obvious delay (~0.1 s) for **[Ir-2]**$^+$ to produce ECL (Fig. 6B). This is because after the reduction of **Ir-1**, the radical anions of **Ir-1**, which carry negative charges are repelled by the working electrode that serves as the cathode. This repulsion could accelerate the radicals to the diffusion layer to react with benzoyl radicals and emit ECL. Exemplar photon and electron flux curves of **[Ir-2]**$^+$ with BPO at 10 Hz pulsing are shown in Fig. S7.

Table 2. Time Interval between the Formation of Cationic and Anionic Radical Species

Method		**Time (s)**
CV-ECL	**Ir-1**_Ann	33.6
	[Ir-2]$^+$_Ann	32.3
	Ir-1_BPO	12.8
	[Ir-2]$^+$_BPO	3.1
Pulsed-ECL at 10 Hz		0.1
Pulsed-ECL at 100 Hz		0.01

Next, we increased the pulsing frequency to 100 Hz to investigate the impact on their ECL behavior. Figs. S8-S11 demonstrate three cycles of current-time with ECL-time curves of 0.5 mM **Ir-1** and **[Ir-2]**$^+$ in annihilation and coreactant processes, respectively. The ECL intensities were further improved because of the smaller time interval (0.01 s) to generate the corresponding radical species. Fewer radicals decayed, and instead meet and react to emit ECL at a pulsing frequency of 100 Hz. Similar observations were found for ECL efficiencies. Compared with ECL efficiencies with 10 Hz pulsing, pulsing at 100 Hz generates higher efficiency, and both are still significantly higher than those collected by the CV scans. This observation can once again be explained by the time interval corresponding to stability of the radicals. For CV-ECL, with a constant scan rate of 0.1 V/s, the time interval depends on their redox potentials, resulting in tens of seconds for radical species to meet and react. For pulsing methods, the time interval of 10 Hz is 0.1 s and that of 100 Hz is 0.01 s, both of which are much shorter than the ones of CVs, leading to the decay of fewer

radical species before they interacted, thus resulting in higher ECL efficiencies. These differences in time intervals depending on the method are summarized in Table 2. The frequency effect originates from the fact that none of the radicals generated in an electrochemistry process for these complexes is stable. As such, shorter time intervals result in fewer decayed radicals and higher ECL efficiency.

Compared with our recent investigation of $[Ru(bpy)_3]^{2+}$[22, 23], the absolute ECL efficiencies of the two iridium complexes are a little lower but comparable in both potentiodynamic scans and potential pulsing processes, indicating that iridium (III) complexes can act as another type of ECL material for practical application.

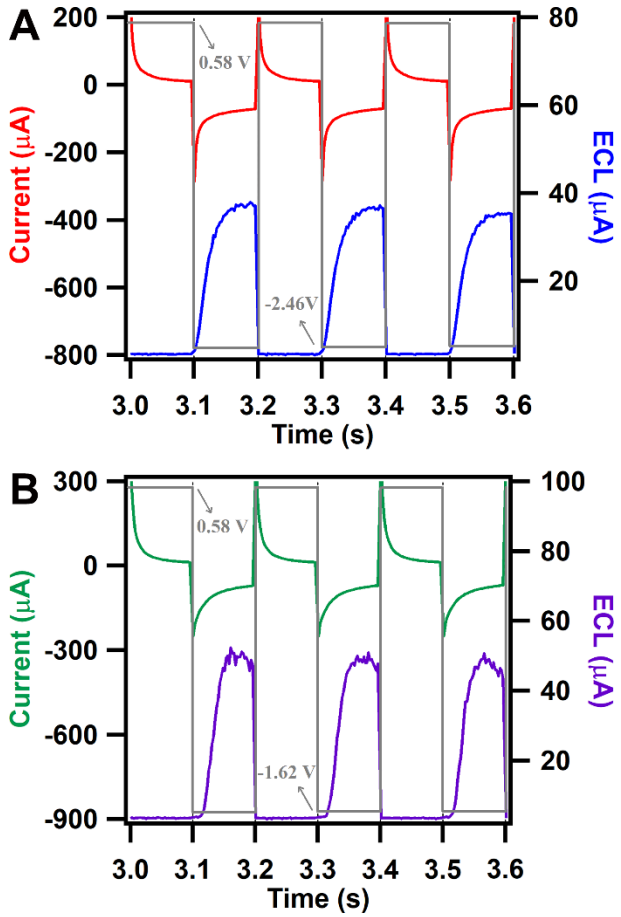

Fig. 6. Three cycles of current-time with the corresponding ECL-time curves of 0.5 mM (A) **Ir-1** and (B) **[Ir-2]**$^+$ (OD=1) with 5 mM BPO as the coreactant during a potential pulsing experiment at 10 Hz frequency. The corresponding applied potentials are indicated in grey.

3.5. Charge effect

The difference in the charge of the complexes may also contribute to the differences in the ECL efficiencies of **Ir-1** and **[Ir-2]**$^+$. For instance, **[Ir-2]**$^+$ is positively charge. During its oxidation, it

forms the radical dications **[Ir-2]$^{2+}$,** which would be repelled into the diffusion layer by the working electrode that was employed as the anode carrying positive charge. During its reduction, neutral radical species **[Ir-2]** would be generated that is neither attracted nor repelled by the working electrode. In comparison, for **Ir-1** that is initially neutral, both the oxidative products **[Ir-1]**$^{+}$ and the reductive products **[Ir-1]**$^{-}$ would be repelled by the working electrodes and the number of radical species in the diffusion layer would increase as a result. A similar analysis can be made for the coreactant ECL route: The radical anions of **Ir-1** would be repelled by the electrode and thus the concentration of this species would increase in the diffusion layer while this would not be the case for the neutral **[Ir-2]**. As such, **Ir-1** should show a higher ECL efficiency compared to **[Ir-2]**$^{+}$. However, whatever is the electrochemistry method, **[Ir-2]**$^{+}$ consistently demonstrates higher ECL efficiencies than **Ir-1** (Table 1), which is due to the higher stability and stronger reactivity of the radicals of **[Ir-2]**$^{+}$ than **Ir-1**. We can therefore conclude that the intrinsic charge of the complex does not materially contribut*e* to the relative ECL efficiencies of these iridium complexes.

3.6. Absolute ECL efficiencies vs. relative ECL efficiencies

We then calculated the relative ECL efficiencies of the two iridium complexes using equation (9) where *x* represents the ECLphore studied and *st* indicates the standard sample $[Ru(bpy)_3]^{2+}$. Note that the concentration of $[Ru(bpy)_3]^{2+}$ is 0.5 mM, which is identical to those of **Ir-1** and **[Ir-2]**$^{+}$. The concentration of BPO remains 5 mM. All the other experimental conditions also remain the same including the working electrode, solvent and supporting electrolyte.

$$\phi_x = \frac{\left(\frac{\int ECL\, dt}{\int current\, dt}\right)x}{\left(\frac{\int ECL\, dt}{\int current\, dt}\right)st} \times \phi_{st} \quad (9)$$

By taking ϕ_{st} as 5%[24], the relative ECL efficiencies of **Ir-1** and **[Ir-2]**$^{+}$ are summarized in Table 1. It is evident that the relative ECL efficiencies determined using this method do not match with the absolute values. Two factors that have significant effect on the ECL efficiencies are the radical stability and radical reactivity, which were not considered during the comparison with $[Ru(bpy)_3]^{2+}$. In other words, the behavior of the radicals of the iridium complexes and $[Ru(bpy)_3]^{2+}$ are different, leading to the divergence in results. Furthermore, as the coreactant ECL efficiencies have never been reported, they are thus not comparable when we assume that the ECL efficiency of $[Ru(bpy)_3]^{2+}$ with BPO is also 5%. Though relative ECL efficiency determination does provide some insights into the relative ECL performance, the absolute ECL efficiency more accurately reflects the electrochemical processes at play and thus provide a more accurate determination of the ECL efficiency.

4. Conclusions

In conclusion, the absolute ECL QEs of two iridium(III) complexes, *fac*-$Ir(ppy)_3$ (**Ir-1**) and $[Ir(ppy)_2(dtbubpy)]^{+}$ (**[Ir-2]**$^{+}$), were determined via annihilation and coreactant processes. For the

ECL generated during potentiodynamic scans, radical stability of the iridium complexes is the key factor influencing the ECL efficiency in the annihilation route, while radical reactivity of the complexes and the radical stability of BPO become dominant in the coreactant pathway. For ECL generation during potential pulsing, the frequency was not modulated and the time interval between radical generation becomes as small as 0.1 s for 10 Hz and 0.01 s for 100 Hz, respectively, resulting in radical reactivity becoming the dominant parameter that affects ECL efficiency. Intermediate charge has little effect on ECL generation from various charge species. Importantly, the behavior of the iridium-based radicals is different from those based on $[Ru(bpy)_3]^{2+}$ and thus it is not appropriate to rely on the relative ECL QE as an accurate predictor of the true ECL QE. We thus advocate the use of absolute ECL QE to assess ECL efficiencies.

Credit authorship contribution statement

Liuqing Yang: Methodology, Investigation, Formal analysis, Data curation, writing-original draft

Jonathan R. Adsetts: Methodology, Investigation, Software, Data curation

Ruizhong Zhang: Methodology, Investigation, Formal analysis

Barbora Balónová: Investigation, Validation

Marta T. Piqueras: Investigation, Validation

Kenneth Chu: Validation

Congyang Zhang: Validation

Eli Zysman-Colman: Supervision, Writing-review & editing

Barry A. Blight: Supervision, Writing-review & editing

Zhifeng Ding: Supervision, Methodology, Validation, Writing-review & editing

Declaration of Competing Interest

The authors declare that they have no known competing financial interests or personal relationships that could have appeared to influence the work reported in this paper.

Acknowledgment

This work is financially supported by Natural Sciences and Engineering Research Council Canada (NSERC, DG RGPIN-2018-06556 and SPG STPGP-2016-493924), Canada Foundation of Innovation/Ontario Innovation Trust (CFI/OIT, 9040) and The University of Western Ontario. The quality service from our Electronic Shop in Chemistry and ChemBioStores is very much

appreciated. The authors thank Dr. Diego Rota Martir for the synthesis of $[Ir(ppy)_2(dtbubpy)]PF_6$ (**[Ir-2]**$^+$). E. Z.-C. is a Royal Society Leverhulme Trust Senior Research fellow (SRF\R1\201089)

Appendix A. Supplementary data

Supplementary data to this article can be found online at https://doi.org/xxx

References

[1] M. Hesari, Z. Ding, Review—Electrogenerated Chemiluminescence: Light Years Ahead, J. Electrochem. Soc. 163 (2016) H3116-H3131.
[2] W. Gu, X. Wang, J. Wen, S. Cao, L. Jiao, Y. Wu, X. Wei, L. Zheng, L. Hu, L. Zhang, C. Zhu, Modulating Oxygen Reduction Behaviors on Nickel Single-Atom Catalysts to Probe the Electrochemiluminescence Mechanism at the Atomic Level, Anal. Chem. 93 (2021) 8663-8670.
[3] W.J. Miao, Electrogenerated chemiluminescence and its biorelated applications, Chem. Rev. 108 (2008) 2506-2553.
[4] H.H. Xing, H.Y. Xia, Y.C. Fan, Y. Xue, C. Peng, J.T. Ren, J. Li, E. Wang, A Solid-State Electrochemiluminescence Sensor Based on Novel Two-Dimensional Ti3C2 MXene, Chemelectrochem 8 (2021) 1858-1863.
[5] Z. Ning, M. Chen, G. Wu, Y. Zhang, Y. Shen, Recent advances of functional nucleic acids-based electrochemiluminescent sensing, Biosens. Bioelectron. 191 (2021) 113462.
[6] L. Hu, Y. Wu, M. Xu, W. Gu, C. Zhu, Recent advances in co-reaction accelerators for sensitive electrochemiluminescence analysis, Chem. Commun. 56 (2020) 10989-10999.
[7] H. Ding, P. Zhou, W. Fu, L. Ding, W. Guo, B. Su, Spatially Selective Imaging of Cell-Matrix and Cell-Cell Junctions by Electrochemiluminescence, Angew. Chem. Int. Ed. 60 (2021) 11769-11773.
[8] C. Ma, S. Wu, Y. Zhou, H.F. Wei, J. Zhang, Z. Chen, J.J. Zhu, Y. Lin, W. Zhu, Bio-Coreactant-Enhanced Electrochemiluminescence Microscopy of Intracellular Structure and Transport, Angew. Chem. Int. Ed. 60 (2021) 4907-4914.
[9] X. Ma, W. Gao, F. Du, F. Yuan, J. Yu, Y. Guan, N. Sojic, G. Xu, Rational Design of Electrochemiluminescent Devices, Acc. Chem. Res. 54 (2021) 2936-2945.
[10] Y. Wang, G. Zhao, H. Chi, S. Yang, Q. Niu, D. Wu, W. Cao, T. Li, H. Ma, Q. Wei, Self-Luminescent Lanthanide Metal-Organic Frameworks as Signal Probes in Electrochemiluminescence Immunoassay, J. Amer. Chem. Soc. 143 (2021) 504-512.
[11] C. Xu, J. Li, S.A. Kitte, G. Qi, H. Li, Y. Jin, Light Scattering and Luminophore Enrichment-Enhanced Electrochemiluminescence by a 2D Porous Ru@SiO2 Nanoparticle Membrane and Its Application in Ultrasensitive Detection of Prostate-Specific Antigen, Anal. Chem. 93 (2021) 11641-11647.
[12] D. Pan, Z. Fang, E. Yang, Z. Ning, Q. Zhou, K. Chen, Y. Zheng, Y. Zhang, Y. Shen, Facile Preparation of WO3-x Dots with Remarkably Low Toxicity and Uncompromised Activity as Co-reactants for Clinical Diagnosis by Electrochemiluminescence, Angew. Chem. Int. Ed. 59 (2020) 16747-16754.
[13] Y.J. Zheng, Z.Q. Ning, D. Pan, D. Han, Y. Xu, S.Q. Liu, Y.J. Zhang, Y.F. Shen, Electrochemiluminescent detection of hNQO1 and associated drug screening enabled by futile redox cycle reaction, Sens. Actuators B Chem. 321 (2020) 128557.
[14] J.M. Wong, R. Zhang, P. Xie, L. Yang, M. Zhang, R. Zhou, R. Wang, Y. Shen, B. Yang, H.-B. Wang, Z. Ding, Revealing crystallization-induced blue-shift emission of a di-boron complex by enhanced photoluminescence and electrochemiluminescence, Angew. Chem. Int. Ed. 59 (2020) 17461-17466.

[15] L. Yang, A.D. Hendsbee, Q. Xue, S. He, C.R. De-Jager, G. Xie, G.C. Welch, Z. Ding, Atomic precision graphene model compound for bright electrochemiluminescence and organic light-emitting diodes, ACS Appl. Mater. Interfaces 12 (2020) 51736-51743.
[16] A. Abdussalam, F. Yuan, X. Ma, F. Du, Y.T. Zholudov, M.N. Zafar, G. Xu, Tris(2,2′-bipyridine)ruthenium(II) electrochemiluminescence using rongalite as coreactant and its application in detection of foodstuff adulteration, J. Electroanal. Chem. 857 (2020) 113752.
[17] Y. Qin, Z. Wang, J. Xu, F. Han, X. Zhao, D. Han, Y. Liu, Z. Kang, L. Niu, Carbon Nitride Quantum Dots Enhancing the Anodic Electrochemiluminescence of Ruthenium(II) Tris(2,2'-bipyridyl) via Inhibiting the Oxygen Evolution Reaction, Anal. Chem. 92 (2020) 15352-15360.
[18] K.N. Swanick, S. Ladouceur, E. Zysman-Colman, Z. Ding, Correlating electronic structures to electrochemiluminescence of cationic Ir complexes, RSC Adv. 3 (2013) 19961-19964.
[19] D. Zhu, Y. Zhang, S. Bao, N. Wang, S. Yu, R. Luo, J. Ma, H. Ju, J. Lei, Dual Intrareticular Oxidation of Mixed-Ligand Metal-Organic Frameworks for Stepwise Electrochemiluminescence, J. Amer. Chem. Soc. 143 (2021) 3049-3053.
[20] X. Zhu, H. Xing, Y. Xue, J. Li, E. Wang, S. Dong, Atom-Anchoring Strategy with Metal-Organic Frameworks for Highly Efficient Solid-State Electrochemiluminescence, Anal. Chem. 93 (2021) 9628-9633.
[21] X. Zhu, Q. Zhai, W. Gu, J. Li, E. Wang, High-Sensitivity Electrochemiluminescence Probe with Molybdenum Carbides as Nanocarriers for alpha-Fetoprotein Sensing, Anal. Chem. 89 (2017) 12108-12114.
[22] J.R. Adsetts, K. Chu, M. Hesari, J. Ma, Z. Ding, Absolute electrochemiluminescence efficiency quantification strategy exemplified with Ru(bpy)3(2+) in the annihilation pathway, Anal. Chem. 93 (2021) 11626-11633.
[23] K. Chu, J.R. Adsetts, J. Ma, C. Zhang, M. Hesari, L. Yang, Z. Ding, Physical Strategy to Determine Absolute Electrochemiluminescence Quantum Efficiencies of Coreactant Systems Using a Photon-Counting Photomultiplier Device, J. Phys. Chem. C 125 (2021) 22274-22282.
[24] N.E. Tokel-Takvoryan, R.E. Hemingway, A.J. Bard, Electrogenerated chemiluminescence. XIII. Electrochemical and electrogenerated chemiluminescence studies of ruthenium chelates, J. Amer. Chem. Soc. 95 (2002) 6582-6589.
[25] C.P. Keszthelyi, N.E. Tokel-Takvoryan, A.J. Bard, Electrogenerated chemiluminescence. Determination of the absolute luminescence efficiency in electrogenerated chemiluminescence. 9,10-Diphenylanthracene-thianthrene and other systems, Anal. Chem. 47 (2002) 249-256.
[26] K. Chu, J.R. Adsetts, S. He, Z. Zhan, L. Yang, J.M. Wong, D.A. Love, Z. Ding, Electrogenerated Chemiluminescence and Electroluminescence of N-Doped Graphene Quantum Dots Fabricated from an Electrochemical Exfoliation Process in Nitrogen-Containing Electrolytes, Chem. Eur. J. 26 (2020) 15892-15900.
[27] J.R. Adsetts, S. Hoesterey, C. Gao, D.A. Love, Z. Ding, Electrochemiluminescence and Photoluminescence of Carbon Quantum Dots Controlled by Aggregation-Induced Emission, Aggregation-Caused Quenching, and Interfacial Reactions, Langmuir 36 (2020) 14432-14442.
[28] L. Yang, D. Koo, J. Wu, J.M. Wong, T. Day, R. Zhang, H. Kolongoda, K. Liu, J. Wang, Z. Ding, B.L. Pagenkopf, Benzosiloles with crystallization-induced emission enhancement of electrochemiluminescence: Synthesis, electrochemistry, and crystallography, Chem. Eur. J. 26 (2020) 11715-11721.
[29] L. Yang, C.R. De-Jager, J.R. Adsetts, K. Chu, K. Liu, C. Zhang, Z. Ding, Analyzing Near-Infrared Electrochemiluminescence of Graphene Quantum Dots in Aqueous Media, Anal. Chem. 93 (2021) 12409-12416.
[30] Z.H. Xu, H. Gao, N. Zhang, W. Zhao, Y.X. Cheng, J.J. Xu, H.Y. Chen, Ultrasensitive Nucleic Acid Assay Based on Cyclometalated Iridium(III) Complex with High Electrochemiluminescence Efficiency, Anal. Chem. 93 (2021) 1686-1692.

[31] S. Voci, R. Duwald, S. Grass, D.J. Hayne, L. Bouffier, P.S. Francis, J. Lacour, N. Sojic, Self-enhanced multicolor electrochemiluminescence by competitive electron-transfer processes, Chem. Sci. 11 (2020) 4508-4515.
[32] B. Balónová, D.R. Martir, E.R. Clark, H.J. Shepherd, E. Zysman-Colman, B.A. Blight, Influencing the Optoelectronic Properties of a Heteroleptic Iridium Complex by Second-Sphere H-Bonding Interactions, Inorg. Chem. 57 (2018) 8581-8587.
[33] B. Balónová, H.J. Shepherd, C.J. Serpell, B.A. Blight, Ir(III) as a strategy for preorganisation in H-bonded motifs, Supramol. Chem. 32 (2019) 1-12.
[34] A. Colombo, C. Dragonetti, V. Guerchais, C. Hierlinger, E. Zysman-Colman, D. Roberto, A trip in the nonlinear optical properties of iridium complexes, Coord. Chem. Rev. 414 (2020) 213293.
[35] A.K. Pal, S. Krotkus, M. Fontani, C.F.R. Mackenzie, D.B. Cordes, A.M.Z. Slawin, I.D.W. Samuel, E. Zysman-Colman, High-Efficiency Deep-Blue-Emitting Organic Light-Emitting Diodes Based on Iridium(III) Carbene Complexes, Adv. Mater. 30 (2018) 1804231.
[36] L. Yang, X. Sun, D. Wei, H. Ju, Y. Du, H. Ma, Q. Wei, Aggregation-Induced Electrochemiluminescence Bioconjugates of Apoferritin-Encapsulated Iridium(III) Complexes for Biosensing Application, Anal. Chem. 93 (2021) 1553-1560.
[37] N.S. Adamson, A.G. Theakstone, L.C. Soulsby, E.H. Doeven, E. Kerr, C.F. Hogan, P.S. Francis, L. Dennany, Emission from the working and counter electrodes under co-reactant electrochemiluminescence conditions, Chem. Sci. 12 (2021) 9770-9777.
[38] Y.Y. Zhou, Y.M. Ding, J.H. Dong, Y.B. Zhao, F. Chen, Y.J. He, Low oxidation potential electrochemiluminescence from novel Iridium(III) complexes comprising N-heterocyclic carbene main ligands containing dibenzothiophene motif, J. Electroanal. Chem. 895 (2021) 115534.
[39] K. King, P. Spellane, R.J. Watts, Excited-state properties of a triply ortho-metalated iridium (III) complex, J. Amer. Chem. Soc. 107 (1985) 1431-1432.
[40] D.R. Martir, C. Momblona, A. Pertegás, D.B. Cordes, A.M.Z. Slawin, H.J. Bolink, E. Zysman-Colman, Chiral Iridium(III) Complexes in Light-Emitting Electrochemical Cells: Exploring the Impact of Stereochemistry on the Photophysical Properties and Device Performances, ACS Appl. Mater. Interfaces 8 (2016) 33907-33915.
[41] M. Hesari, Z. Ding, Spooling electrochemiluminescence spectroscopy: development, applications and beyond, Nat. Protoc. 16 (2021) 2109-2130.
[42] Y. Ohsawa, S. Sprouse, K.A. King, M. DeArmond, K. Hanck, R. Watts, Electrochemistry and spectroscopy of ortho-metalated complexes of iridium (III) and rhodium (III), J. Phys. Chem. 91 (1987) 1047-1054.
[43] D. Bruce, M.M. Richter, Green electrochemiluminescence from ortho-metalated tris(2-phenylpyridine)iridium(III), Anal. Chem. 74 (2002) 1340-1342.